NRIAG JOURNAL OF ASTRONOMY AND GEOPHYSICS
2019, VOL. 8, NO. 1, 131–143
https://doi.org/10.1080/20909977.2019.1627634

Integrating magnetic and stratigraphic data to delineate the subsurface features in and around new Galala City, Northern Galala Plateau, Egypt

Maha Abdelazeem[a], Mohamed Sobhy Fathy[b] and Mohamed Mostafa Khalifa[a]

[a]Department of Geomagnetism and Geoelectricity, National Researchn Istitute of Astronomy and Geophysics (NRIAG), Helwan, Egypt; [b]Geology Department, Faculty of Science, Tanta University, Tanta, Egypt

ABSTRACT

The Egyptian Government is developing a new city, Galala, above the Northern Galala Plateau, western side of Gulf of Suez between Ain Sukhna and Zafarana. The aim of the study is integrating magnetic and stratigraphic data to delineate the subsurface features beneath the New Galala City, in order to avoid the possible geological hazards. The stratigraphic succession in the study area consists of Precambrian basement complex overlain unconformably by Phanerozoic sequence. The Phanerozoic sequence composed mainly of siliciclastic-dominated rocks superimposed by carbonate-dominated rocks. The carbonate-dominated rocks cover most surface area, whilst the siliciclastic-dominated rocks exposed along eastern and southern foot slope of the Northern Galala Plateau. The observed palaeo-karst surfaces, fissures, caves, sink-holes and fault zones within carbonate rocks may cause some geological hazards in the study area. The total intensity aeromagnetic map was subjected to un-prescribed structural index 3D-Euler Deconvolution (ED), the tilt angle derivative (TDR) and the power spectrum in order to estimate both trends and source depths. The source depths range from 500 m to 4000 m, which result from the Precambrian basement complex. However, the trends of encountered structural elements are mainly NE–SW, NW–SE, NNW–SSE and E–W directions.

ARTICLE HISTORY
Received 19 February 2019
Revised 12 May 2019
Accepted 1 June 2019

KEYWORDS
Magnetic; stratigraphic sequence; karstification; New Galala city; FFT; TDR and ED

1. Introduction

The Northern Galala Plateau extends for about 80 km from east to west and reaches the highest point of 1260 m above sea level. It is bounded by the narrow coast of the Gulf of Suez and extends westward to join Gebel Mokattam, near the Nile Valley. Wadi Ghewibba and Wadi Araba border the plateau from the north and south, respectively.

Galala is a new promising city developed by the Egyptian government in the empty Eastern Desert on the Northern Galala Plateau, Western side of Gulf of Suez. The city is considered as the second biggest project in Egypt, after the New Suez Canal project. It occupies an area of 19,000 acres and will include several hotels, service and medical projects, King Abdullah University, and a new road linking Ain Sukhna to Zafarana through Galala Mountain (Figure 1). However, the area under investigation lies between latitudes 28° 45` & 29° 45` N and longitudes 31° 45` & 32° 45` E (Figure 2).

Since Schweinfurth (1885) recorded the Paleozoic fossils in Wadi Araba, the area attracted many authors to investigate the geological setting of the area. Sadek (1926) studied the geology and geography of the area between Gebel Ataqa and Northern Galala plateau. He introduced Khashm El Galala Formation for the Jurassic rocks exposed at Khashm El Galala area. Most of the rock units of the Paleozoic – Mesozoic sequences of the studied area (e.g. Rod El Hamal, Aheimer, Qiseib, Malha, … . formations) were introduced by Abdallah and El Adindani (1965), Abdallah et al., (1965), Awad and Abdallah (1966), and El Akkad and Abdallah (1971). A revision of the lithostratigraphic classification of the Permo-Carboniferous outcrops of the Gulf of Suez region carried out by Kora (1998). Bandel & Kuss (1987) delineated the depositional environment of the pre-rift sediments at the Northern and Southern Galala plateau, which ranged from fluvial to open marine environments.

Two structural phases were detected by Moustafa and Khalil (1995) in the Gulf of Suez region. The Late Cretaceous phase of deformation, folds with NE-SW oriented axes were formed in northern Egypt as a result of convergence between Africa and Eurasia and the closure of the Neotethys. The second early Miocene phase, deformation NW-oriented normal faults was formed as a result of the opening of the Suez Rift. The carbonate platform in the studied area formed as a result of the initial topography that was controlled by the tectonic uplift of the Northern Galala/Wadi Araba Syrian Arc structure (Scheibner et al. 2001).

CONTACT Maha Abdelazeem maazeem03@hotmail.com Department of Geomagnetism and Geoelectricity, National Researchn Istitute of Astronomy and Geophysics (NRIAG), Helwan, Egypt

Figure 1. Location of a new Galala and the current projects. a, b, c and d show the development of the new roads and compounds in Galala City, above Northern Galala plateau, Egypt.

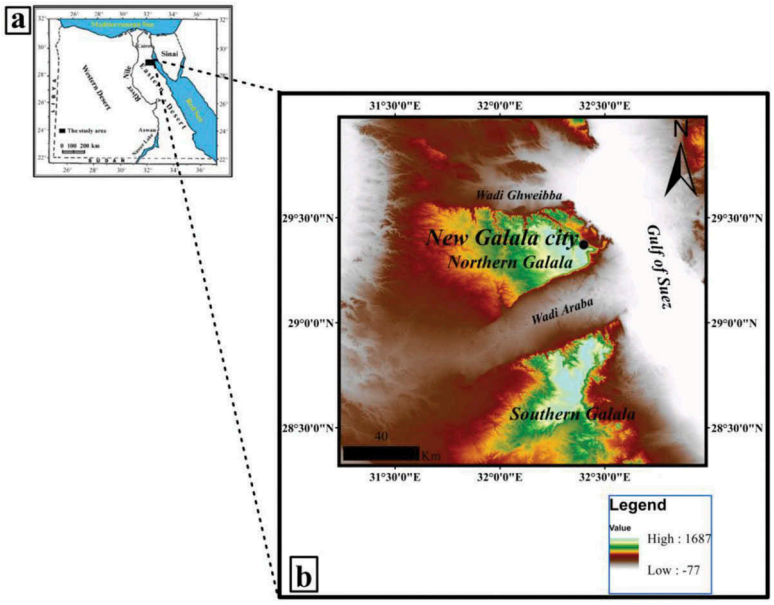

Figure 2. (a) Location map of the New Galala city above Northern Galala plateau, west the Gulf of Suez, Egypt, and (b) Shows the topographic features and geomorphic frameworks around the city.

Saada 2016 carried out the magnetic method to estimate the depth of basement rocks in wadi Araba area with application of some filters. The depth estimation was applied using different techniques ranges from about 200 to 4000 m. Moreover, these techniques indicate that wadi Araba is highly affected by the Gulf of Suez rifting system and the Syrian Arc folding system.

The present work integrates magnetic and stratigraphic data to delineate the subsurface structures, which affect the lithological succession beneath the New Galala City, in order to avoid the geological hazards while planning the new urban areas. During three field trips, the stratigraphic setting, lithologic characters, sedimentary structures, and fossil content are established about the exposed sequences around the new Galala city. Geophysical investigation is carried out by analyzing and interpreting aeromagnetic data.

2. Stratigraphic sequence

The stratigraphic succession beneath the New Galala City starts with the Precambrian complex of igneous

and metamorphic rocks at the base, which is, unconformably, overlain by Phanerozoic rocks. The Phanerozoic sequence is composed mainly of siliciclastic-dominated rocks of Cambrian to Lower Cretaceous age and carbonate-dominated rocks of Upper Cretaceous to Eocene age. The stratigraphic units of the Phanerozoic succession are briefly described from base to top as follows.

2.1. Combrian-lower cretaceous siliciclastic-dominated rocks

Cambro-Ordovician sediments in the studied are represented by unexposed Araba and Naqus formations. The Araba Formation rests unconformably over the basement complex and conformably followed by Naqus Formation. They composed mainly of varicolored, massive, pebbly and cross-bedded sandstones with reddish-grey mudstone intercalations.

A Carboniferous Rod El Hamal Formation is the first exposed rock unit in the studied area where its lower surface is unexposed and unconformably overlain by Qiseib Formation. This formation consists mainly of alternating five siliciclastic-carbonate-dominated units of about 260 m thick. It is exposed along the southern cliff of the Galala plateau and Wadi Araba (Figure 3). Aheimer Formation (Upper Carboniferous-Lower Permian) attains a thickness of 250 m in the type locality at Wadi Aheimer within the eastern cliff of the Galala plateau (Abdallah and El Adindani 1965) and extends to Ain Sukhna area (Figure 3). It is composed mainly of thick-bedded fossiliferous (foraminifers, brachiopods and corals) limestones. This carbonate deposits are sandwiched between two siliciclastic deposits from multicoloured,

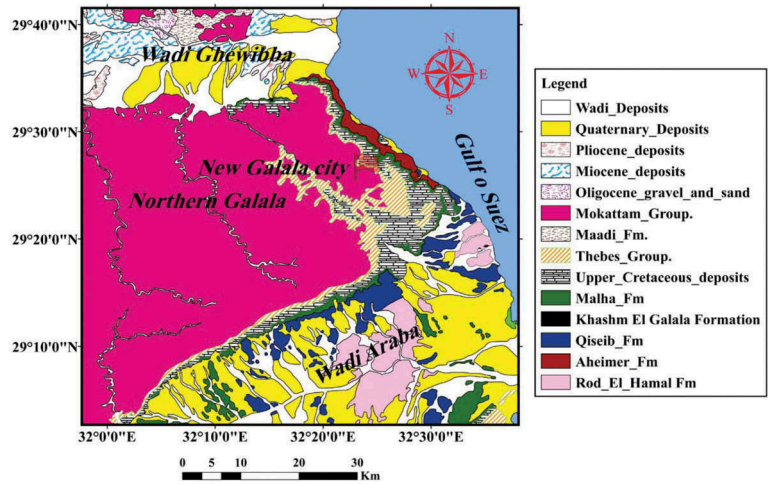

Figure 3. Geological map of the area around New Galala city, Northern Galala plateau, Gulf of Suez, Egypt (*modified after* Conoco 1987).

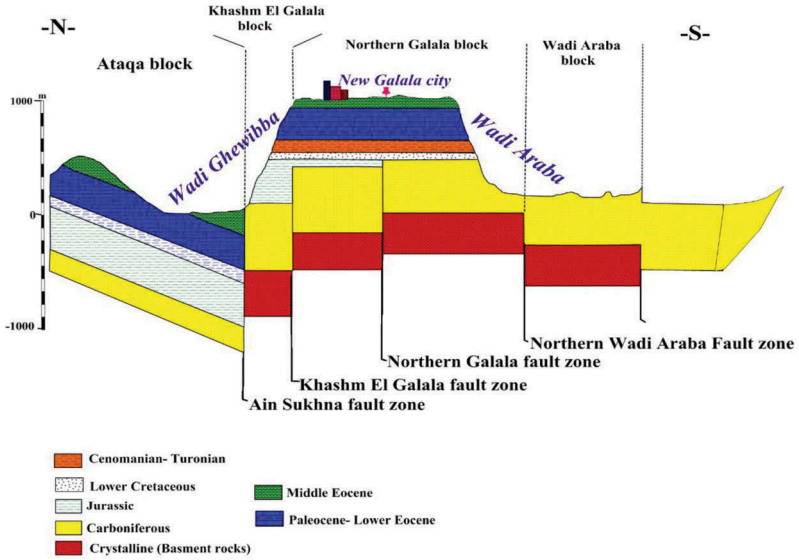

Figure 4. A sketch showing the structural and the stratigraphic setting of the lithological succession beneath the New Galala city, Northern Galala plateau, Egypt (*modified after* Bandel and Kuss 1987).

cross bedded, friable sandstones alternating with a number of fossiliferous shale and dolostone beds.

The Permo-Triassic reddish brown clastic sediments (46 m thick) are exposed along Wadi Qiseib around the Port Sokhna Resort introduced by Abdallah *et al.*, (1965) as a Qiseib Formation. It lies conformably upon the Rod El Hamal Formation and/or Aheimer Formation, and it is unconformably overlain by the Lower Cretaceous sandstones of the Malha Formation. Figure 5(a) shows the effect E-W fault in the Qiseib Formation, exposed around the new roads of the southern parts of the New Galala city.

Khashm El Galala Formation consists mainly of intercalations of cross-bedded sandstones, silty shale with limestones and dolomite beds of the middle Jurassic age. It attains a thickness of 250 m exposed at its type locality at Khashm El Galala area, near the north-eastern side of the plateau as described by Sadek (1926). Lower Cretaceous Malha Formation composed of 150 m from non-marine friable, cross-

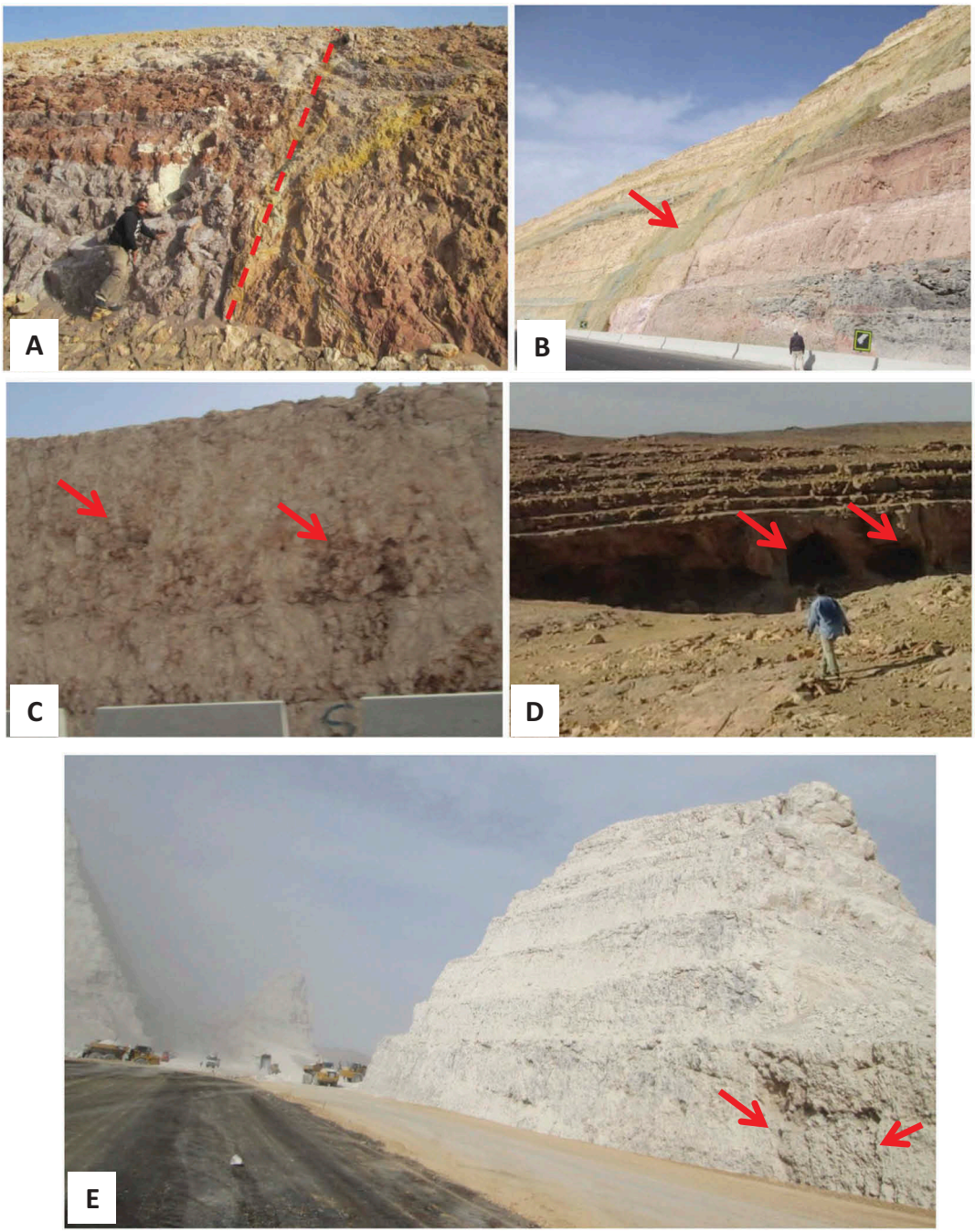

Figure 5. Field photographs show the different stratigraphic exposures at the New Galala City. A) E-W fault zone within Permo-Triassic Qiseib Formation, southern part of the city, B)Arrow refers NW-SE fault zone within Lower Cretaceous Malha Formation exposed in the side of new Galala highway, C)Arrows refer to voids and paleokarst sediments within Upper Cretaceous carbonate rocks (Adabiya Formation), D)Arrows refer to caves result from karstification within carbonates of the Lower Eocene Thebes Formation, E)Arrows refer to NE-SW fault zone in Middle Eocene Mokattam Formation, while background shows the drilling process of the new Galala highway, northern part of the city.

bedded, coarse to fine-grained sandstones and kaolinitic mudstone interbeds (Figure 5(b)) with occasional marine layers at the upper part. Malha Formation conformably underlies Galala Formation and unconformably overlies the Permo-Triassic red beds of the Qiseib Formation.

2.2. Upper Cretaceous–Eocene carbonate-dominated rocks

Upper Cretaceous succession in the studied area represented by Galala and Adabiya formations. A distinctive greenish yellow, fossiliferous sediments above sandstones of the Malha Formation outcrops along Galala escarp represented by Galala Formation, which underlies unconformably the Adabiya Formation. The Adabiya Formation measured and described through the new exposure around new roads of the Galala city with a thickness reaches to 40 m of limestone and dolostone intercalations. A paleokarst surface was noted in the upper part of this formation (Figure 5(c)). It might have been developed when the carbonate platform was exposed to weathering due to small drop in the sea-level and/or synsedimentary block faulting (uplifting) in the studied area.

Through field trips, the stratigraphic successions of the Paleocene Maghra El Bahari and Southern Galala formations are described and measured around some new construction buildings of the Galala City. They attain about 260 m from a thick bedded to massive fossiliferous and dolomitic limestones with thin layers of marl and sandstone intercalations. Most of the bedrocks located to the southeast of the Galala city are covered with carbonate rocks of the Thebes Formation of Lower Eocene age (Figure 3). The chalky limestone and chalk with chert nodules and bands are the main component of the present formation. The most extensive case of karstification is found at the top of the carbonate rocks of the formation. It covers the whole exposed surfaces and extends deeply downward up to 10 m causing many caves and sinkholes (Figure 5(d)). Humid climate favours karstification of exposed carbonate platforms during sea-level low-stands (Flügel 2004).

As shown in Figure 3, most of the topmost part of the Northern Galala represented by the carbonate rocks of the Mokattam Formation (Middle Eocene age), which unconformably overlies the Thebes Formation with noticeable paleokarst surface. This formation is well marked by the limestone beds that carry the characteristic *Nummulites gizehensis* (Said, 1962). Karstification, dolomitisation and dissolution are the common diagenetic processes affectedthe carbonate rocks of the Mokattam Formation, especially along the main fault zone in the studied area (Figure 5(e)). According to Palmer (1991), karst landscapes in which dissolution of bedrock by water is one of the dominant geomorphic processes occupy 10%-20% of the Earth's land area. Nearly all major surface karst features owe their origin to internal drainage, subsidence, and collapse triggered by the development of underlying caves.

3. Magnetic data processing and interpretation

3.1. Acquisition and enhancement of aeromagnetic data

The aeromagnetic data covers the study area is prepared by digitising four maps of scale 1:50,000 (Figure 6). These represent part of the aeromagnetic survey of the Eastern Desert, compiled and carried out by (Aero-Service 1984). The total aeromagnetic map was reduced to the pole in the frequency domain (Figure 7) with inclination angle (41.99°) and declination angle (2.33°). The map relief is about 448 nT.Qualitatively, this indicated non-homogeneous texture of the magnetic sources in the study area. Three different anomaly zones can be distinguished based on the anomaly amplitude/intensity, these are **A**: anomalies with high intensity (>42,336 nT), **B** anomalies less than 42,336 and greater than 42,250 nT, and **C** anomalies of lower intensity (< 42,250 nT). Distribution of these anomalies reveals that the lower intensity anomalies are concentrated at the central and the western parts of the studied area, these are followed by much greater intensities **B** and **A** at the borders of the area. The boundary of different magnetic signature zones is marked by dashed lines. This may represent possible contact/faults crossing the area.

3.2. Depth estimation from aeromagnetic data

Quantitative interpretation of the magnetic data requires estimating the expected depths to the magnetic sources in the study area. This can be achieved by applying different filters: like power spectrum, Euler Deconvolution and tilt angle filter. The depth to both shallow and deep-seated magnetic units are determined using 2D radially average power spectrum (Figure 8). The Fast Fourier Transform (FFT) is applied to the RTP magnetic data to calculate a two-dimensional power spectrum curve (Telford et al. 1990).

Figure (8) shows that depths of magnetic sources in the area under study can be classified into two categories: the shallow sources population with depth reaches to 378 m, and the deep sources population reaches to 4390 m. The resulted cut-off frequency 0.0396 1/K, analogous to depth 4390 m, is used to calculate the regional field (Figure 9). The low magnetic anomalies are located in the centre and in the western parts (**C**), and high magnetic anomalies (high zones)

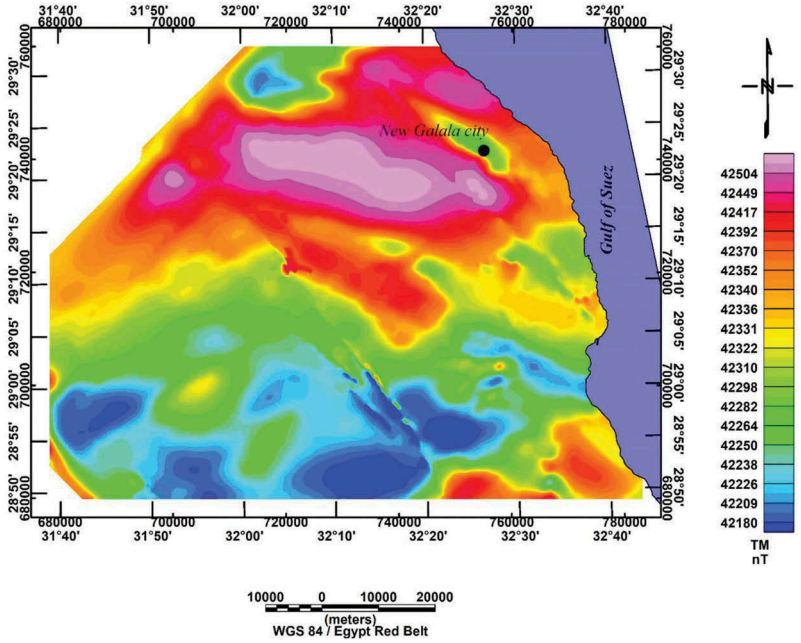

Figure 6. Total magnetic intensity map of the study area.

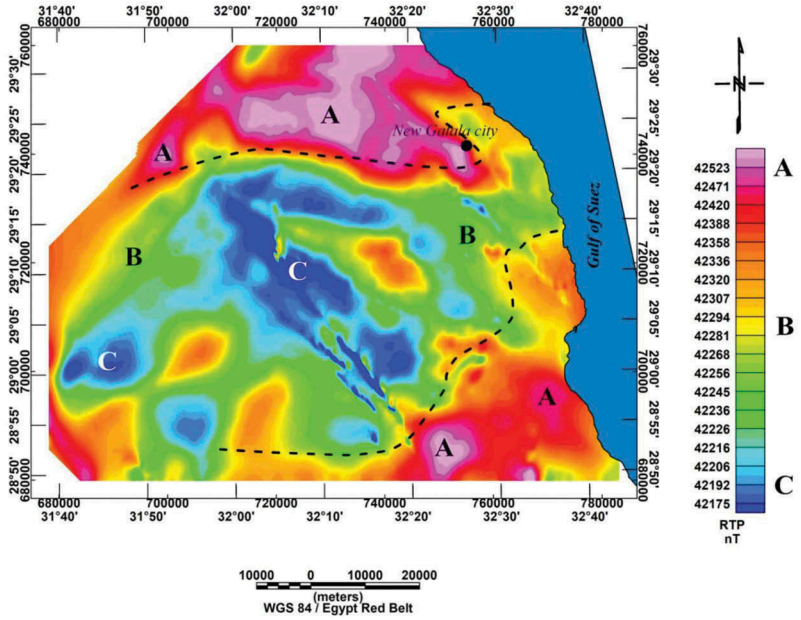

Figure 7. Reduced to Pole (RTP) magnetic anomaly map of the study area (effect of Skewedness is cancelled).

cover the northern part and the southeastern part (**A**). While the intermediate anomalies cover the northeastern and the central zone surrounding the Low region (**C**). The most remarkable feature in the near-surface field (residual magnetic field) is the linear anomaly in the central part and trending NW-SE and bounding the large low magnetic regional zone at the central part of the study area. This may be due to suture/contact zone in this area. Moreover, it is characterised by the presence of system of the magnetic narrow closures distributed all over the study area with local variations in both the amplitude and frequencies.

3.3. The tilt-depth method

Miller and Singh (1994); Verduzco et al. (2004); Salem et al. 2007b and Golshadi et al. (2016) developed the tilt derivative method (TDR), which provides a simple and rapid technique to estimate the depth to the magnetic basement for large areas. The method depends on the determination of the tilt angle θ which takes the form (Nabighian 1972):

$$\theta = \tan^{-1}\left(\frac{\partial M/\partial z}{\partial M/\partial h}\right) \quad (1)$$

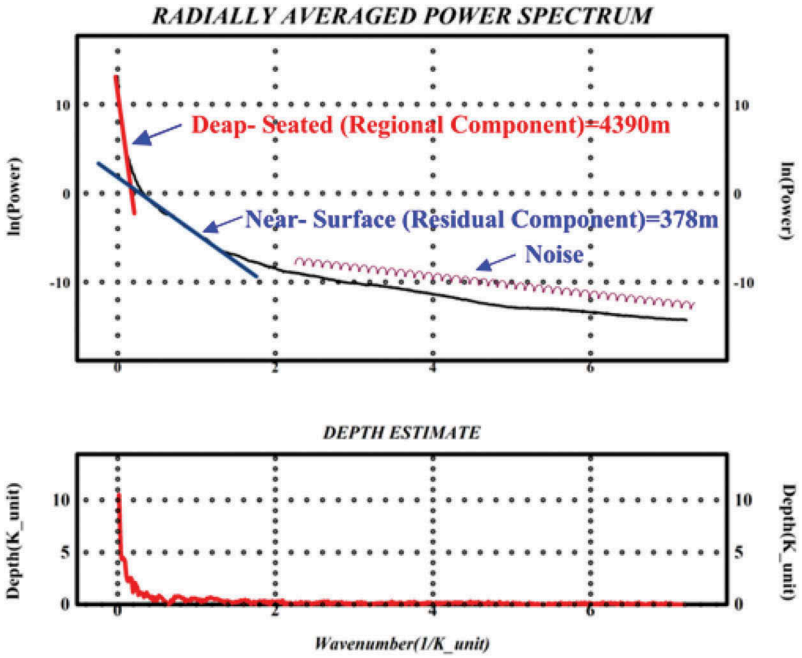

Figure 8. Depths to deep and shallow structures as estimated from 2D radially average power spectrum.

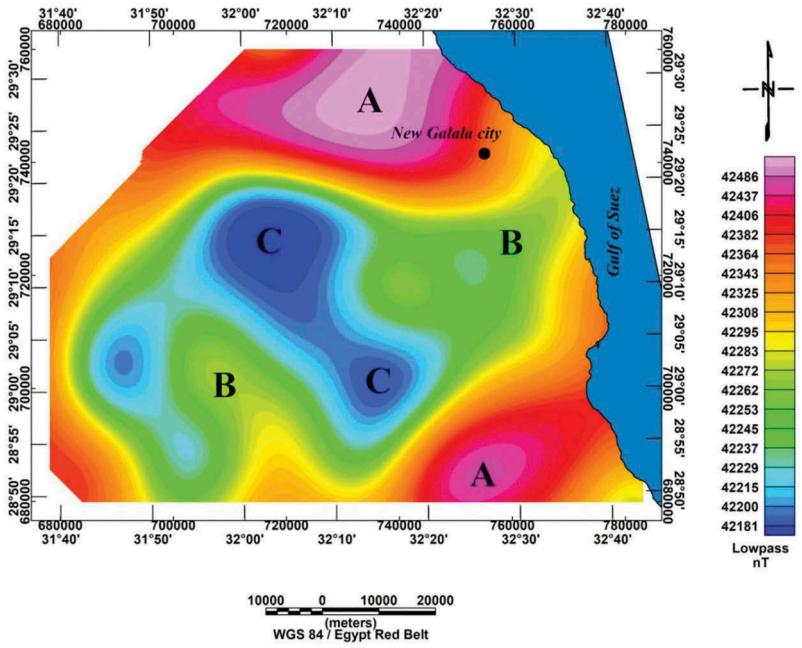

Figure 9. Regional (low pass) magnetic anomaly map of the study area. Observe the central low magnetic anomaly trending NW-SE.

where, $\frac{\partial M}{\partial h} = \sqrt{\left(\frac{\partial M}{\partial x}\right)^2 + \left(\frac{\partial M}{\partial y}\right)^2}$ and $\frac{\partial M}{\partial x}, \frac{\partial M}{\partial x}, \frac{\partial M}{\partial z}$ are the first order derivatives of the magnetic field M in the x, y and z directions. The Tilt angle, θ, is measured in either radians or degrees.

Salem et al. 2007a, used the general expressions published by Nabighian (1972) for the vertical and horizontal derivatives of the magnetic field over contacts located at a horizontal location of h= 0 and at a depth of Z_c (depth to contact). They showed that (equation 1) could be rewritten as:

$$\theta = \tan^{-1}\left(\frac{h}{Z_c}\right) \tag{2}$$

where h is the horizontal distance from the horizontal location of the contact and Z_c is the depth to the top of the contact. This equation indicates that when the Tilt is 0° (h= 0) this is the location of the contact and when the Tilt value is 45° and −45° then h= Z_c or h = – Z_c, respectively. The perpendicular distance h between the zero contour and other Tilt contours

can be used but require an associated coefficient to equate them to Z_c. Tilt derivative map for the study area is shown in (Figure 11), and the clusters of depths that estimated from Tilt map are plotted on RTP map and is shown in (Figure 12).

Figure 11 confirms the linear feature centred in the area and trending NW-SE (Figure 10). The depth to the possible contact ranges from 500 to 2000 m showing that the origin of this vertical contact is deep and cutting the sedimentary section in the region. Figure 12 shows that the depths to the northern (**A**) anomaly is less than 500 m indication shallow source. This is similar to the contact at the eastern limb.

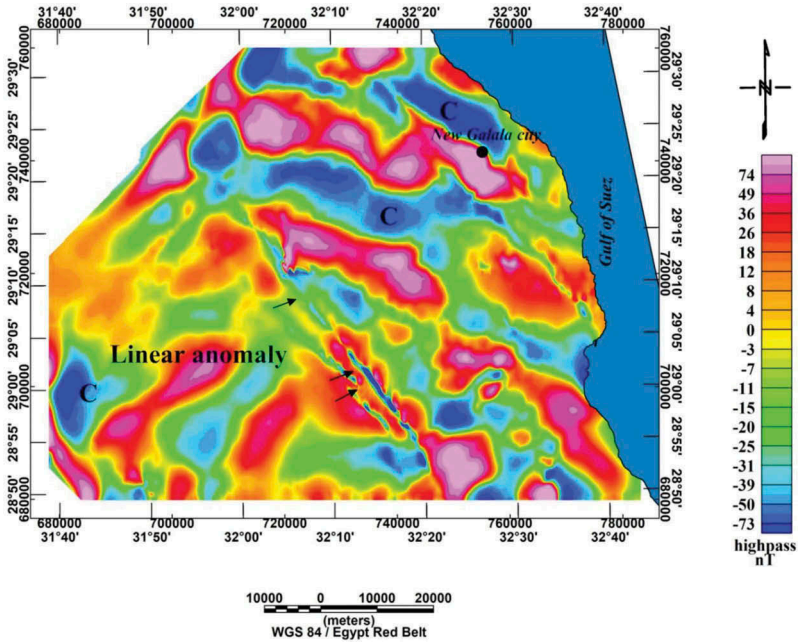

Figure 10. Residual (high pass) magnetic anomaly map of the study area. Arrows indicate the location of possible linear features.

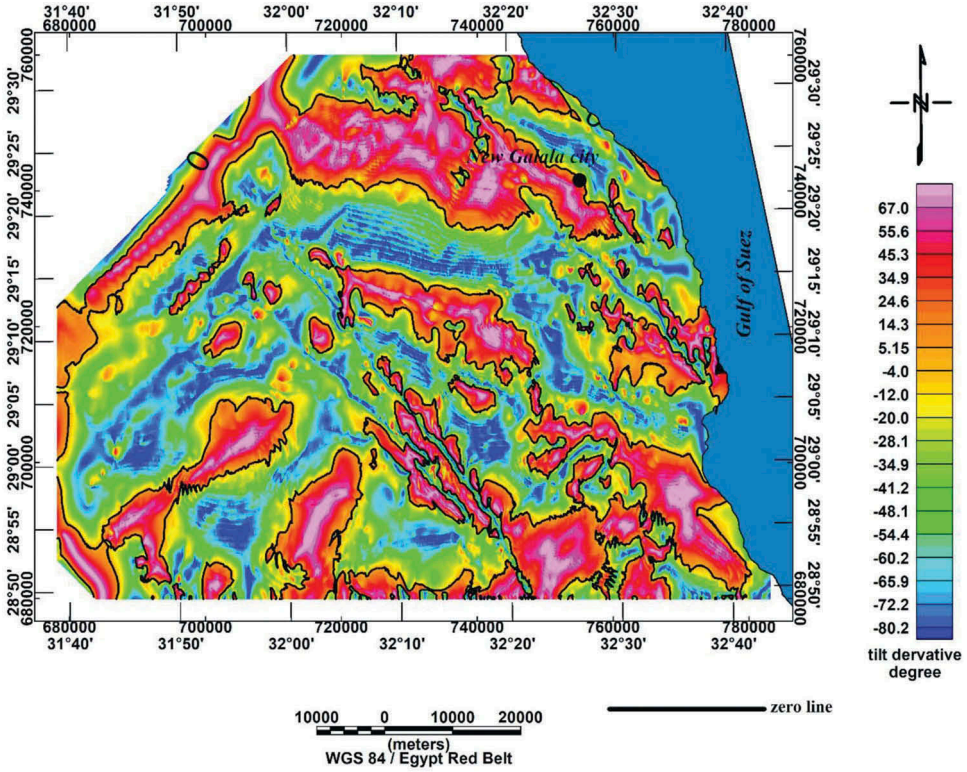

Figure 11. The tilt derivative map calculated from the RTP field of the area with only one contour for angle zero, representing the locations of magnetic contacts.

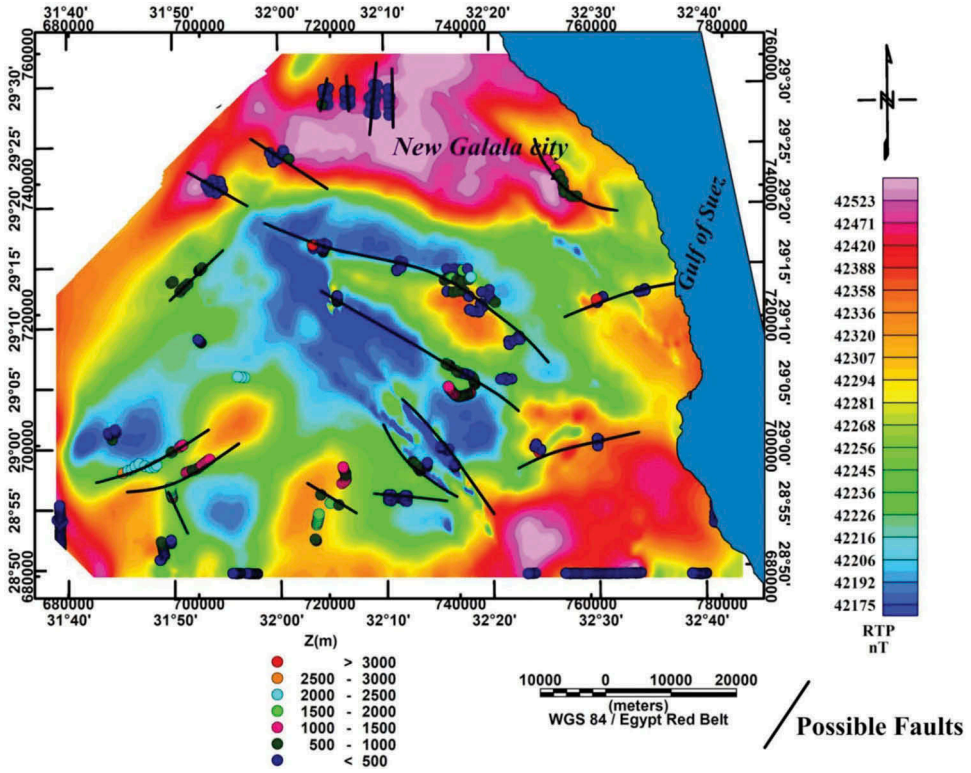

Figure 12. Depths to vertical contacts as estimated from the tilt derivative field posted on the RTP map of the study area.

3.4. 3D Euler deconvolution (ED) and magnetic source identification

Thompson (1982), introduced the Euler deconvolution technique (ED) for profile data analysis. It was later extended to gridded data (Reid et al. 1990). Euler's homogeneity equation, when accounting for a base level for the background field, can be written as:

$$(x - x_0)\frac{df}{dx} + (y - y_0)\frac{df}{dy} + (z - z_0)\frac{df}{dz} = NF \quad (3)$$

where the homogeneous function f is the observed field at location (x, y, z), which is caused by a source at location(x_0, y_0, z_0), and N, physically, is a measure of the rate of decay of the field with the distance and, geophysically, is the structural index (SI) that is related directly to the shape of the causative source.

The above-described conventional Euler deconvolution cannot determine the existed structural elements in the area. One has to determine manually the specific structural index (SI) to analyze, using the geologic experience. In the present section (3D analysis), the pilot technique, proposed by Stravrev and Reid (1997) and Gerovska and Araúzo-Bravo (2003), was applied to interpret the aeromagnetic anomalies of Wadi Nu'man, Makkah Al Mukarammah, KSA (Gobashy and Al-Garni 2008), assuming a linear background with un-prescribed structural index based on the properties of the differential similarity transformation (DST). The un-prescribed Euler Deconvolution method, simply results are the position of the source and the source kind.

We applied such method to the RTP (aeromagnetic data) of Galala plateau, focusing on the calculated depths and structural indices associated with the different clusters resulted from the different stages, and use it to infer relationships between the resulted lineation and the geologic units in the study area. The target is to deduce the common structural elements in the area magnetically. The accepted solutions are distributed in 19 groups (Figure 13). Table 1 summarises the solutions clusters, their confident and average positions and also the structures' indices. Table 2 clarifies only the depths, structures' indices and structure types. The average depth of all groups is 916 m, and the average structure index is 0.5, indicating a magnetic contact model (Reid et al. 1990). Cluster index G10 represents the most common structural element (110 solution points). It has an average depth of 637.47 m and average structure index 1.12, indicating sill/dyke.

3.5. Structural interpretation of the magnetic field data

The structural lineaments of the prospect area of study were interpreted from the RTP, tilt angle, and 3D-Euler depth maps (Figure 14). These structure systems are statistically analyzed and plotted in the form of rose diagrams as shown in (Figure 14).

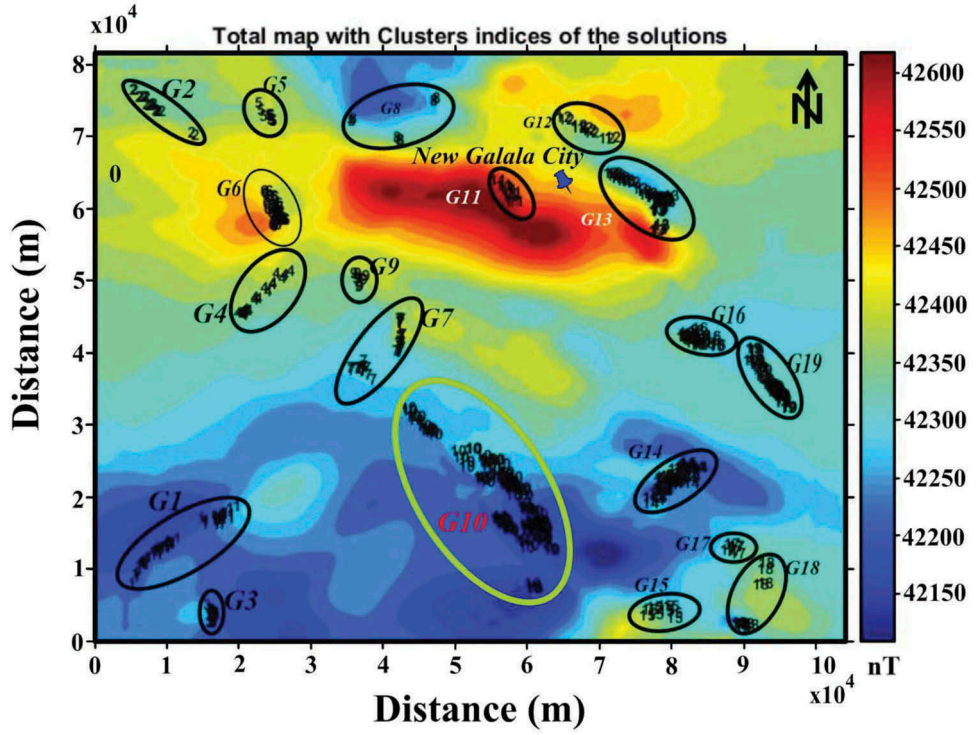

Figure 13. Final cluster indices of the accepted solutions, posted on TMI map.

Table 1. Results of 3D-Euler deconvolution analysis for the study area.

Cluster index	Num Poi	Xave	Xcon	Yave	Ycon	Zave	Zcon	Nave	Ncon
1	49	14,395	5860.4	11,613	9508.6	1490.9	1182.5	0.2557	0.3781
2	16	74,101	3786.8	7578.9	5172.5	310.71	370.16	0.2586	0.4981
3	24	3855.2	1298.5	15,658	537.09	539.32	390.08	0.4319	0.4312
4	20	47,716	4540	22,081	4774.7	812.54	780.7	0.7313	1.029
5	10	72,797	1729.7	23,363	1617.1	292.02	388.42	0.193	0.408
6	38	59,538	2899.1	24,409	1480.8	1163.9	1157.2	0.5589	0.7437
7	45	40,786	4697.4	40,028	5029	656.62	772.12	0.6581	0.7056
8	7	71,888	6087.5	41,012	11,540	939.55	483.1	0.1849	0.3772
9	8	50,239	1588.1	35,937	1281.3	490.63	621.42	0.2565	0.3909
10	110	20,185	10,645	55,516	9621.1	637.47	700.62	1.12	1.7481
11	8	62,281	2445.2	55,927	1933.8	1239.9	1184.4	0.2264	0.4444
12	9	70,979	2366.6	66,550	5179.6	1218.9	504.27	0.3054	0.3896
13	44	61,393	4176.6	75,442	4808.3	1224.1	904.37	0.3118	0.6199
14	38	22,628	3028.7	78,878	3808.9	1001.4	1090.5	1.0241	1.3372
15	9	4394.7	1364.5	77,058	3398.5	1505.7	863.09	0.4356	0.7488
16	25	42,054	1300.1	81,879	2797	385.16	437.06	0.4012	0.4606
17	6	13,045	1320.2	86,987	1245.6	1591.5	1021.1	0.3296	0.4001
18	13	4648.8	7424.3	89,123	3255	1250.6	1049.2	0.7357	1.2337
19	46	35,633	4466.5	92,263	2953.5	645.3	511.84	1.0517	1.0222

NumPoi: Number of points.
Xave: Average x value.
Xcon: Confidence interval for variable X.
Yave: Average Y value.
Ycon: Confidence interval for variable Y.
Zave: Average z value.
Zcon: Confidence interval for variable Z.
Nave: Average estimated structural indices for each cluster.
Ncon: Confidence interval for estimated structural indices N.

The trend analysis of this diagram shows two predominant structural trends having variable intensities and lengths (Tables 3 and 4). These are the NW-SE, and E–W trends, representing the most predominant tectonic trends affecting the investigated area as deduced from the magnetic point of view. However, the other minor structural trends appearing on the rose diagrams such as the N–S, NE, ENE, WNW, NNW, NNE, and ENE are of less significance in this area. These trends are observed and measured in the exposed stratigraphic sequences (Figure 5) during the field trips. Moreover, the average depth as calculated from the 3D Euler is found to be 916 m and the average structure index is 0.5, indicating a magnetic contact model as a common structural element affecting the study area.

Table 2. Average depths (Zavr) in meters and structural indices (Navr) for different groups.

Cluster index	Zave	Nave	Predicted causative structure
G1	1490.9	0.25,567	Contact
G2	310.71	0.25,858	Contact
G3	539.32	0.43,191	Contact
G4	812.54	0.73,128	Contact/thin sheet
G5	292.02	0.19,302	Contact
G6	1163.9	0.55,893	Contact/thin sheet
G7	656.62	0.6581	Contact/thin sheet
G8	939.55	0.18,492	Contact
G9	490.63	0.25,648	Contact
G10	637.47	1.12	(Sill/dike)
G11	1239.9	0.2264	Contact
G12	1218.9	0.30,535	Contact
G13	1224.1	0.31,182	Contact
G14	1001.4	1.0241	(Sill/dike)
G15	1505.7	0.43,558	Contact
G16	385.16	0.40,116	Contact
G17	1591.5	0.3296	Contact
G18	1250.6	0.73,569	Contact/thin sheet
G19	645.3	1.0517	(Sill/dike)

4. Conclusions and recommendations

The area under study is a high human activity area. The study aim is mainly to describe the subsurface structural setting of the lithological succession beneath the new-constructed Galala city and its surroundings to avoid the expected geological hazards that may affect the city in the future. The stratigraphic sequence in the study area made up of basement complex which covered unconformably by a thick sedimentary succession. The unexposed basement complex consists mainly from igneous and metamorphic rocks of late to post Precambrian age. The sedimentary sequence ranges in age from Cambrian to Eocene. Except unexposed Cambro-Ordovician sediments, field investigations and discussion of all exposed rock units have been undertaken.

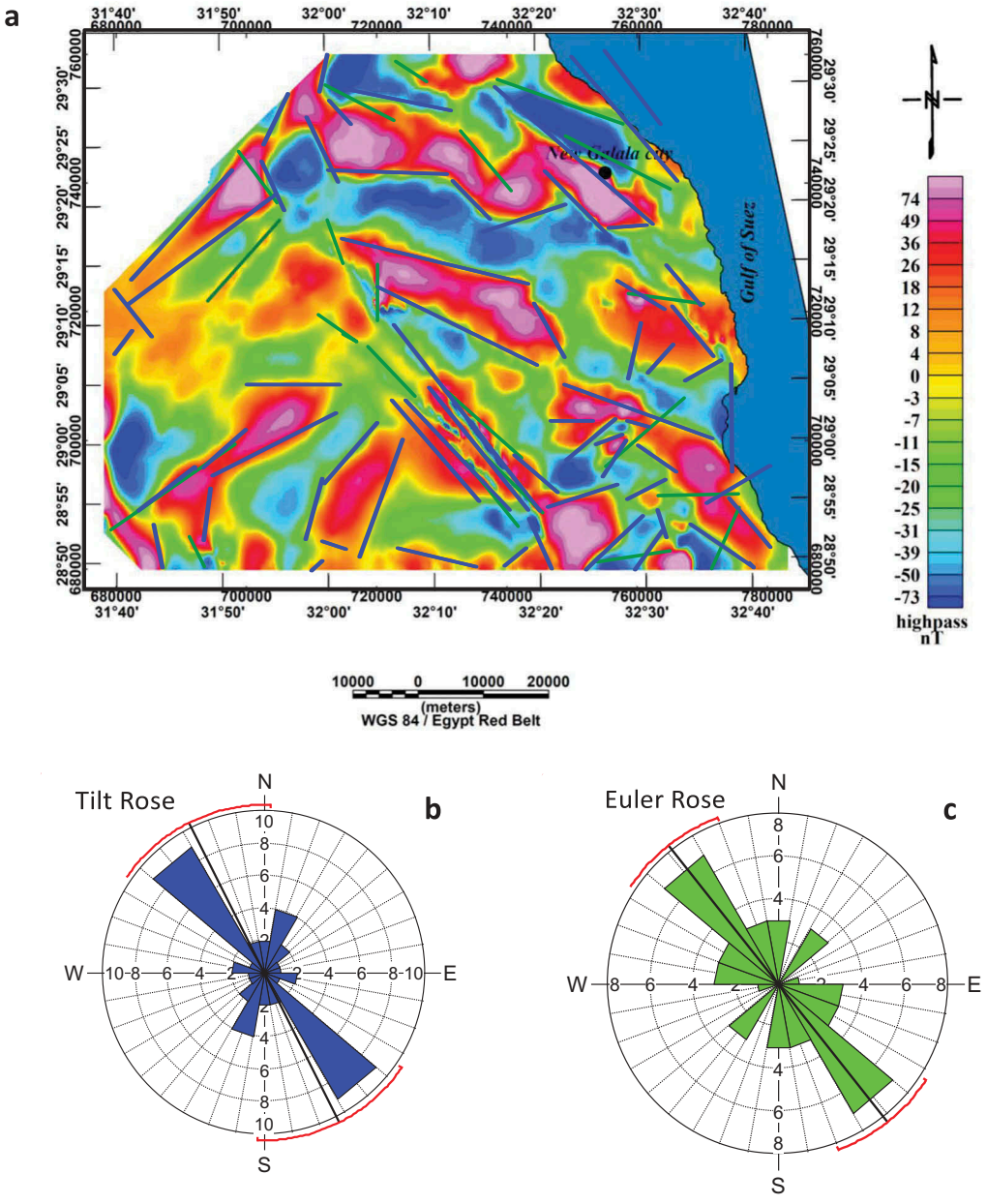

Figure 14. Main Structural Lineaments as deduced from different filters. a) Lineaments posted on the residual map, b) Rose diagram of the lineaments inferred from TDR filter and c) Rose diagram of the lineaments inferred from 3D-Euler filter.

Table 3. Statistical Analysis of interpreted trends from TDR map.

Trend	N	L	N%	L%
N-S	37	528,278	57.81	65.57
NNE-SSW	5	51,446	7.81	6.39
NE-SW	12	133,952	18.75	16.63
ENE-WSW	8	79,304	12.5	9.84
E-W	2	12,732	3.13	1.58
Total	64	805,712	100	99

N: Number of faults.
L: Average length.
N%: Percentage of fault number.
L%: Percentage of length w.r.t. the total lengths.

Table 4. Statistical Analysis of interpreted trends from 3D-Euler map.

Trend	N	L	N%	L%
N-S	17	204,716	73.91	69.4
NNE-SSW	1	9954	4.35	3.37
NE-SW	2	33,179	8.7	11.25
ENE-WSW	1	22,534	4.35	7.64
E-W	2	24,608	8.7	8.34
Total	23	294,991	100	100

N: Number of faults.
L: Average length.
N%: Percentage of fault number.
L%: Percentage of length w.r.t. the total lengths.

The Paleocene-Eocene carbonate rocks (e.g. Thebes and Mokattam formations) form the most prominent lithologic units exposed in the New Galala city. Such rocks cover a great area of the uppermost surface of the Galala plateau. Beside the tectonic movements affected in the Gulf of Suez region, the present carbonate rocks suffered from various diagenetic processes for a long time. Hence, the carbonate rocks have different caves, joints, sinkholes and karst which might be case vital problem in the building process. Karst is common to areas underlain by carbonate bedrock, which are more easily dissolved than other rocks by a weak, natural acid formed by the mixture of water and carbon dioxide. The dissolving process is enhanced along the many fractures found within the bedrock, and over time this has created a unique subsurface plumbing network, and we must take some precautions in engineering design in large buildings to avoid such potential problems. Moreover, shallow seismic and ground penetrating radar (GPR) studies are recommended to be established before constructions.

The most predominant structural trends affecting the New Galala city area as deduced from the magnetic method are NW-SE, and E–W trends, with minor trends as the N–S, NE, ENE, WNW, NNW, NNE, and ENE. The most common structural element affecting the area is the magnetic contact model (SI = 0.5). These are relatively of shallow depth to top (about 900 m). The new Galala city is affected by Groups 11, 12 and 13 of clustered contact-like sources trending NW-SE, i.e red sea trend. With average depth of 1227 m (Table 2). This is confirmed from both 3D Euler and tilt derivative filters. Such trends are also observed and measured in the exposed stratigraphic sequences (Figure 5).

Disclosure statement

No potential conflict of interest was reported by the authors.

References

Abdallah AM, El Adindani A, Fahmy N. 1965. Stratigraphy of the lower mesozoic Rocks, Western side of the Gulf of Suez, Egypt. Cairo (Egypt). Egypt Geologicl Survey and Mineral Research Department Paper No. 27.

Abdallah AM, El Adindani B Stratigraphy of upper Paleozoic rocks western side of the Gulf of Suez. Geol. Surv. Egypt. Paper No. 25, p.18.

Aero-Service. 1984 April. Final operational report of airborne magnetic-radiation survey in the Eastern Desert, Egypt. For the Egyptian General Petroleum Corporation (EGPC), Cairo, Egypt Vol. Six. Houston (Texas, U. S. A.): Aero-Service Division, Western Geophysical Company.

Awad GH, Abdallah AM. 1966. Upper cretaceous, Eastern Desert, with emphasis on neighboring areas. J Geol UAR. 10(2):125–144.

Bandel K, Kuss J. 1987. Depositional environment of the pre-rift sediments: galala heights (Gulf of Suez, Egypt). Berl Geowiss Abh A. 78:1–48.

Conoco C. 1987. Geological map of Egypt 1:500,000. Cairo: The Egyptian General Petroleum Corporation.

Egypt (abstract). In: 6th Arab Petroleum Conference, Baghdad; 39, p.B–3.

El Akkad S, Abdallah AM. 1971. Contribution to geology of Gabal Ataqa area. Ann Geol Surv Egypt. 1:21–42.

Flügel E. 2004. Microfacies of carbonate rocks: analysis, interpretation and applications. Heidelberg: Springer; p. 976.

Gerovska D, Araúzo-Bravo MJ. 2003. Automatic interpretation of magnetic data based on Euler deconvolution with unprescribed structural index. Comput Geosci. 29 (8):949–960.

Gobashy MM, Al-Garni MA. 2008. High resolution ground magnetic survey (HRGM) for determining the optimum location of subsurface dam in Wadi Nu'man, Makkah Al Mukarammah, KSA. J King Abdulaziz Univ Earth Sci. 19:57–83.

Golshadi Z, Ramezanali AK, Kafaei K. 2016. Interpretation of magnetic data in the Chenar-e Olya area of Asadabad, Hamedan, Iran, using analytic signal, Euler deconvolution, horizontal gradient and tilt derivative methods. Boll Geofis Teorica Appl. 57(4):329–342.

Kora M. 1998. The Permo-Carboniferous outcrops of the Gulf of Suez region, Egypt stratigraphic classification and correlation. In S. Crasquin-Soleau, A. Izar, O. Vaslet & P. De .Wever (Eds.), Peri-Tethys: stratigraphic correlations 2. Geodiversitas. 20(4):701–721.

Miller HG, Singh V. 1994. Potential field tilt -a new concept for location of potential field sources. J Appl Geophys. 32:213–217.

Moustafa AR,Khalil MH. 1995. Superposed deformation in the northern Suez rift, Egypt: relevance to hydrocarbons exploration. J Pet Geol. 18:245–266. doi:10.1111/jpg.1995.18.issue-3

Nabighian MN. 1972. The analytic signal of two-dimensional magnetic bodies with polygonal cross-section: its properties and use for automated anomaly interpretation. Geophysics. 37:507–517. doi:10.1190/1.1440276

Palmer A. 1991. Origin and morphology of limestone caves. Geol Soc Am Bull. 103:1–21.

Reid AB, Allsop JM, Granser H, Miliett AJ, Somerton WI. 1990. Magnetic inter-pretations in three dimensions using Euler deconvolution. Geophys. 55:80–91.

Saada SA. 2016. Edge detection and depth estimation of Galala El Bahariya Plateau, Eastern Desert-Egypt, from aeromagnetic data. Geomech Geophys Geo-Energy and Geo-Resour. 2(1):25–41.

Sadek H. 1926. The geography and geology of the district between Gebel Ataqa and El Galala El Bahariya (Gulf of Suez). Egypt: Geol. Surv. Min. Res. Dept.; p. 120.

Said, R. 1962. The geology of Egypt. Amsterdam: Elsevier; p. 377.

Salem A, Williams S, Fairhead D, Smith R, Ravat D. 2007a. Interpretation of magnetic data using tilt-angle derivatives. Geophysics. 73(1):L1–L10.

Salem A, Williams S, Fairhead JD, Ravat D, Smith R. 2007b. Tilt-depth method: A simple depth estimation method using first-order magnetic derivatives. Leading Edge. 26(12):1502–1505.

Scheibner C, Marzouk AM, Kuss J. 2001. Maastrichtian-early eocene litho-biostratigraphy and palægeography of the northern Gulf of Suez region, Egypt. J Afr Earth Sci. 32(2):223–255.

Schweinfurth G. 1885. Sur la découverte d'une fauna Paléozoique dans le Grès d'Egypte. Bull Inst Egypt. 6 (2):239–255.

Stravrev P, Reid A. 1997. Euler deconvolution of gravity anomalies from thick contact/fault structures with extended negative structural index. Geophysics. 75:151–158.

Telford W, Geldart L, sheriff R. 1990. Applied geophysics. Library of Congress Cataloging-in-publication Data. 2nd ed. Cambridge Univ. Press; p. 660.

Thompson DT. 1982. EULDPH—a technique for making computerassisted depth estimates from magnetic data. Geophysics. 47:31–37.

Verduzco B, Fairhead JD, Green CM, Mackenzie C. 2004. New insights into magnetic derivatives for structural mapping. Leading Edge. 23:116–119.